



Stability Issues of the VLHC Rings

K.Y. Ng

Fermi National Accelerator Laboratory, P.O. Box 500,
Batavia, IL 60510*

(March 2001)

Abstract

Beam stability issues of the VLHC rings in Phase 1 and Phase 2 are reviewed. For accelerator rings of circumference 232 km and beam pipe radius of the order of 1 cm, the impedance of the vacuum chamber is dominated by the resistive wall. The most dangerous instabilities are the single-bunch transverse mode coupling instability and the transverse coupled bunch instability driven by the resistive wall at sub-revolution frequency. Scaling is studied concerning the thresholds of these instabilities and the dominance of the resistive wall impedance as the size of the accelerator increases.

Based on a talk given at the VLHC Stability Workshop
SLAC, March 21-23, 2001.

*Operated by the Universities Research Association, Inc., under contract with the U.S. Department of Energy.

1 THE RINGS, INJECTION, AND RF

The present very-large-hadron-collider (VLHC) design consists of two phases [1]. In Phase 1, bunches are injected from the Tevatron into the low-field rings at 900 GeV and are accelerated to 20 TeV. In Phase 2, bunches from the low-field rings are extracted at 10 TeV and injected into the high-field rings and accelerated to 87.5 TeV. Low-field implies the reaching of 1.96 Tesla while high-field implies 10 Tesla. The rings of both phases are chosen to be of the same size, $2\pi R = 231.727$ km in circumference, and same rf frequency. In order to have shorter bunches, the rf frequencies in both phases are chosen 9 times higher than that of the Tevatron, so that the bunches in the VLHC will be separated by 9 rf buckets. The rf harmonic is $h = 9h_{\text{T}}R/R_{\text{T}} = 369432$, where $h_{\text{T}} = 1113$ is the rf harmonic of the Tevatron and $R_{\text{T}} = 1.0$ km is its mean radius. The rf voltage has been chosen to be $V_{\text{rf}} = 50$ MV. However, after injection into the high-field rings, V_{rf} has to be raised to 200 MV so that acceleration can be accomplished within the designed time interval.

In order to avoid or reduce the possibility of longitudinal and transverse single bunch instabilities, the rms bunch area of bunches inside the VLHC buckets are chosen as $A = 2.0$ eV-s, very much larger than the $A_{\text{T}} = 0.359$ eV-s rms bunch area [2] of the Tevatron bunches at 900 GeV. However, with $V_{\text{rf}} = 50$ MV, the maximum energy spread and bucket area are, respectively,

$$\left[\frac{\Delta E}{E} \right]_{\text{bucket}} = \sqrt{\frac{2eV_{\text{rf}}}{\pi h |\eta| E}} = 2.09 \cdot 10^{-3} , \quad (1.1)$$

$$A_{\text{bucket}} = \frac{8}{\omega_0} \sqrt{\frac{2eV_{\text{rf}} E}{\pi h |\eta|}} = 5.01 \text{ eV-s} , \quad (1.2)$$

where $\eta = 2.91 \cdot 10^{-5}$ is the slip factor of the VLHC rings in both phases, $f_0 = \omega_0/(2\pi) = 1.294$ kHz their revolution frequency, and $E = 900$ GeV the injection energy. This bucket is definitely too small for the rms 2 eV-s bunch. In the discussions below, we assume that the bunches in the low-field rings injected from the Tevatron will be of rms bunch area 0.359 eV-s. By the way, the Tevatron rf has its maximum voltage at 1 MV only, the bunch length being too long and the momentum spread too small to fit the VLHC buckets at injection. Thus, the Tevatron bunches must be shortened by either a bunch rotation or the installation of a higher rf voltage before the transfer to the VLHC is possible. Some relevant rf and beam parameters of the VLHC rings are listed in Table 1 for convenience.

Table 1: Parameters of the VLHC rings in Phase 1 and Phase 2, at injection and storage modes. For the last row, see Sec. 5.

	PHASE 1		PHASE 2		
	Injection	Storage	Injection	Storage	
Rings and RF					
Circumference $C = 2\pi R$	231.727	231.727	231.727	231.727	km
Energy E	1.0	20.0	10.0	87.5	TeV
Bunch separation	9	9	9	9	buckets
Rf harmonic h	369432	369432	369432	369432	
Rf voltage V_{rf}	50	50	50	200	
Slip factor	$2.190 \cdot 10^{-5}$	$2.190 \cdot 10^{-5}$	$2.190 \cdot 10^{-5}$	$2.190 \cdot 10^{-5}$	
Synchrotron tune ν_s	$8.46 \cdot 10^{-3}$	$1.79 \cdot 10^{-3}$	$2.54 \cdot 10^{-3}$	$1.72 \cdot 10^{-3}$	
Max. energy spread	$2.09 \cdot 10^{-3}$	$4.44 \cdot 10^{-4}$	$6.27 \cdot 10^{-4}$	$4.24 \cdot 10^{-4}$	
Bucket area	5.013	23.631	16.71	98.86	eV-s
Betatron tune ν_β	214	214	214	214	
Beams					
Bunch frequency	53.105	53.105	53.105	53.105	MHz
Bunch filling	90%	90%	90%	90%	
Number of bunches	36943	36943	36943	36943	
Number per bunch N_b	$2.48 \cdot 10^{10}$	$2.48 \cdot 10^{10}$	$0.90 \cdot 10^{10}$	$0.90 \cdot 10^{10}$	
rms bunch area	0.359	2.00	2.00	2.00	eV-s
rms bunch length σ_ℓ/σ_τ	6.03/0.201	6.55/0.219	7.79/0.260	3.21/0.107	cm/ns
rms energy spread σ_δ	$6.31 \cdot 10^{-4}$	$1.46 \cdot 10^{-4}$	$2.45 \cdot 10^{-4}$	$6.81 \cdot 10^{-5}$	
Freq. at bunch mode					
$m = 0, f_{(0)}$	0.507	0.467	0.393	0.955	GHz
$m = 1, f_{(1)}$	1.015	0.934	0.785	1.910	GHz
$m_{\text{eff}} = 0.304, f_{(m_{\text{eff}})}$	0.169	0.156	0.131	0.318	GHz

A bunch excited by forces in the vacuum chamber oscillates in the longitudinal phase space in modes describable by the radial mode parameter n_r designating n_r radial nodes and the azimuthal mode parameter m designating $|m|$ azimuthal nodes. For a given m , the most easily excited radial mode is $n_r = |m|$ and only these radial modes will be included in the discussion below. Almost distribution independent, the spectrum for the mode designated by $m \neq 0$ peaks at frequency

$$f_{(m)} \approx \frac{|m| + 1}{2\tau_L} , \quad (1.3)$$

where τ_L is the *total* length of the bunch in time. In Gaussian distribution, we approximate it by the 95% length $\tau_L = 2\sqrt{6}\sigma_\tau$, where σ_τ is the rms bunch length. Actually, the spectrum of this mode is nonzero only at the m -th synchrotron sidebands of, respectively, the revolution harmonics for longitudinal discussion and the betatron tune lines for transverse discussion. For $m = 0$, the spectrum has a frequency spread from $-f_{(0)}$ to $+f_{(0)}$ with $f_{(0)}$ given by Eq. (1.3). Both $f_{(0)}$ and $f_{(1)}$ are listed in Table 1. Note that these frequencies for the VLHC bunch modes are in the GHz range.

2 RESISTIVE WALL

The longitudinal impedance of the wall of a *cylindrical* beam pipe of radius b is, at angular frequency ω or harmonic n ,

$$\left[\frac{Z_{\parallel}}{n} \right]_{\text{wall,cyl}} = [\text{sgn}(\omega) + j] \frac{R\rho}{b\delta_1} |n|^{-1/2} , \quad (2.4)$$

where ρ is the resistivity of the beam pipe wall and

$$\delta_1 = \sqrt{\frac{2\rho}{\omega_0\mu}} \quad (2.5)$$

is the skin depth at the revolution harmonic and μ the magnetic permeability. The VLHC beam pipes for the low-field rings are warm with an elliptical cross section of radii $h = 9$ mm and $w = 14.0$ mm. The longitudinal impedance is given by

$$\left[\frac{Z_{\parallel}}{n} \right]_{\text{wall}} = \left[\frac{Z_{\parallel}}{n} \right]_{\text{wall,cyl}} F_L \quad (2.6)$$

with $b = h$, while the transverse impedance is

$$[Z_{V,H}]_{\text{wall}} = \frac{2R}{h^2} \left[\frac{Z_{\parallel}}{n} \right]_{\text{wall,cyl}} F_{V,H} , \quad (2.7)$$

with $|n|^{-1/2}$ replaced by $|n - \nu_{\beta}|^{-1/2}$. In above, the form factors are $F_L = 0.938$, $F_V = 0.821$, and $F_H = 0.408$, for this particular elliptic beam pipe. The beam pipes for the high-field rings are at 80° to 100°K and are circular in cross section with a radius of $b = 1$ cm. These are computed for a stainless steel beam pipe ($\rho = 7.40 \cdot 10^{-7}$ $\Omega\text{-m}$ at all temperatures), an aluminum beam pipe ($\rho = 2.65 \cdot 10^{-8}$ $\Omega\text{-m}$ at all temperatures) and a copper beam pipe ($\rho = 1.70 \cdot 10^{-8}$ $\Omega\text{-m}$ at room temperature, $1.60 \cdot 10^{-9}$ $\Omega\text{-m}$ at 80°K). The results are tabulated in Table 2.

Power dissipated at the wall of the beam pipe by M bunches each containing N_b protons is

$$P = \Gamma\left(\frac{3}{4}\right) M \left[\frac{N_b e c}{2\pi} \right]^2 \left[\frac{Z_0 \rho}{2} \right]^{1/2} \frac{1}{\sigma_{\ell}^{3/2} b} , \quad (2.8)$$

where $\Gamma\left(\frac{3}{4}\right) = 1.225416702$ is the Gamma function at $\frac{3}{4}$, and the beam pipe has been approximated to be cylindrical with radius b . Note that the power loss is proportional to $\sigma_{\ell}^{-3/2}$ where $\sigma_{\ell} = \sigma_{\tau} c$ is the rms bunch length and c the velocity of light. As is displayed in Table 2, the power loss in each aluminum beam pipe is 0.13 to 0.11 W/m in Phase 1 and 0.012 to 0.044 W/m in Phase 2. For each copper beam pipe, the power loss is 0.011 to 0.092 W/m in Phase 1 and 0.003 to 0.011 W/m in Phase 2. However, for each stainless steel beam pipe, the power loss reaches 0.70 to 0.61 W/m in Phase 1 and 0.062 to 0.24 W/m in Phase 2.

In the VLHC, the resistive wall impedances of the beam pipe dominate because of its large size and small pipe radii. At a fixed frequency[†] $\omega/(2\pi)$, the wall impedances scale as

$$\left[\frac{Z_{\parallel}}{n} \right]_{\text{wall}} \propto \frac{1}{h} \sqrt{\frac{R}{\omega}} \quad \text{and} \quad [Z_{\perp}]_{\text{wall}} \propto \frac{1}{h^3} \sqrt{\frac{R^3}{\omega}} . \quad (2.9)$$

where R is the radius of the ring. On the other hand, the inductive parts of the impedances of the beam position monitors (BPMs), for example, scale as

$$\left[\frac{\text{Im } Z_{\parallel}}{n} \right]_{\text{BPM}} \propto \frac{1}{\sqrt{R\omega}} \quad \text{and} \quad [Z_{\perp}]_{\text{BPM}} \propto \frac{\sqrt{R}}{h^2 \omega} , \quad (2.10)$$

[†]Looking at a fixed revolution harmonic, the right side of each equation in Eqs (2.9) and (2.10) should be multiplied by a factor of \sqrt{R} .

where we have assumed that the betatron tune and therefore the number of BPM sets scale as \sqrt{R} . The contributions of the BPMs are plotted alongside with the contributions of the resistive wall in Fig. 1. We see that the contributions of the BPMs are about an order of magnitude smaller than those of the resistive wall, even if the cold copper pipes are taken as reference. The derivation of the BPM impedances is given in the Appendix.

3 POTENTIAL-WELL DISTORTION

The bunch of the prescribed length σ_τ and energy spread σ_E listed in Table 1 will match the rf bucket set up at the voltage of $V_{\text{rf}} = 50$ MV (or 200 MV for Phase 2 at storage). In the presence of an inductive impedance $\mathcal{I}m Z_{\parallel}/n$, the particles inside a bunch see an additional force proportional to the gradient of the particle distribution. Providing that the bunch is short, a beam particle at a time advance τ with respect to the synchronous particle sees a potential drop or voltage of

$$V_{\text{ind}} = \frac{eN_b}{\sqrt{2\pi}\omega_0\sigma_\tau^2} \frac{\mathcal{I}m Z_{\parallel}}{n} \frac{\tau}{\sigma_\tau}, \quad (3.11)$$

which is to be subtracted from the rf voltage supplied by the klystron. Thus, for an inductive impedance at the rf harmonic, this induced voltage counteracts the supplied rf voltage. The bunch shape will be distorted and its length increased. As an illustration, we evaluate this voltage distortion at the 95% of the bunch or $\tau = \sqrt{6}\sigma_\tau$. As shown in Table 2, this inductive voltage, V_{ind} , can be as large as 5 MV for a stainless steel beam pipe, but is less than 1 MV for the aluminum pipe and copper pipe. The low-field beam pipe will be made of aluminum while the high-field beam pipe will be of stainless steel coated internally with copper. Thus, the bunch shape will not be affected much by the inductive wall. In other words, potential-wall distortion is of no importance here.

4 LONGITUDINAL MODE-COUPLING

For only motion in the longitudinal phase space, mode $m = 0$ represents static motion like the potential-well distortion that we discussed before. The next modes are the dipole mode $m = 1$, quadrupole mode $m = 2$, etc. In the presence of coupling impedance,

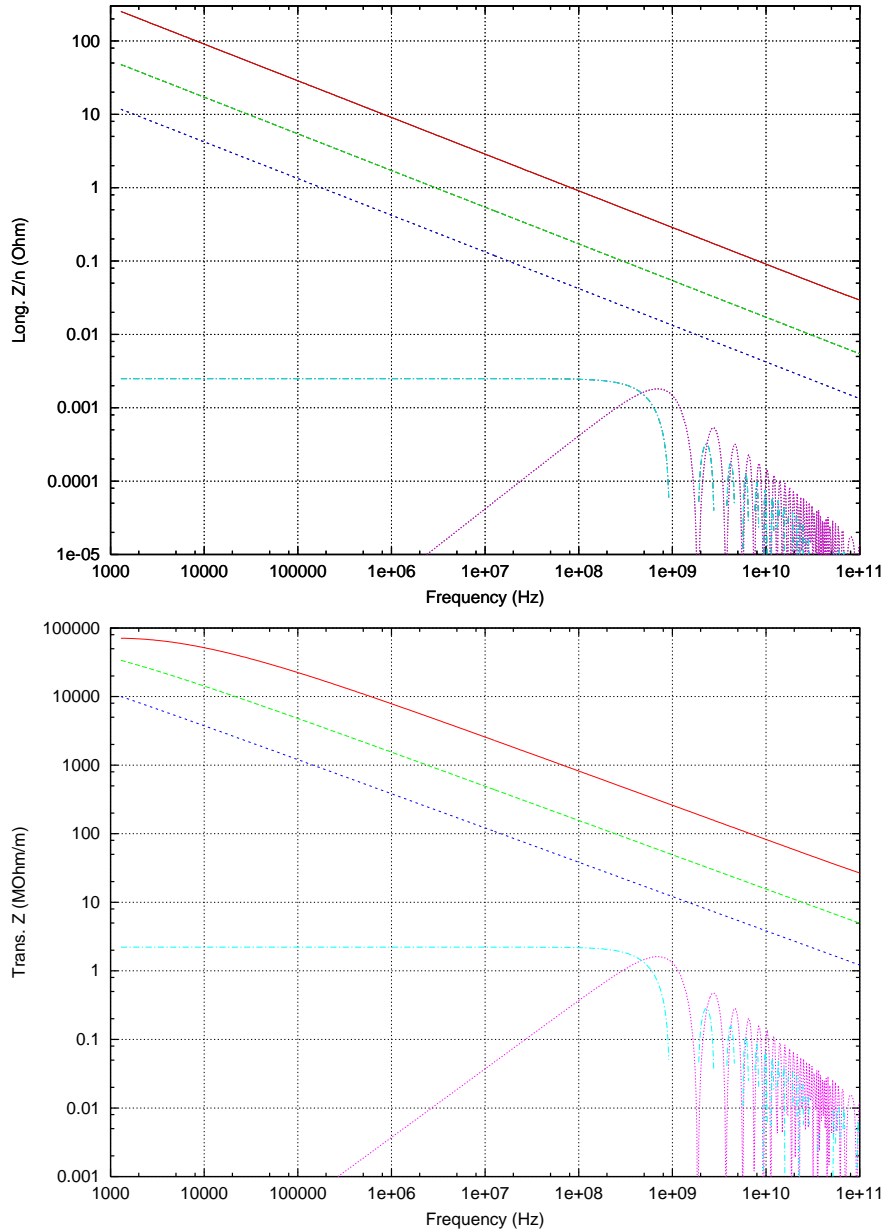


Figure 1: Longitudinal impedance Z_{\parallel}/n (upper plot) and transverse impedance (lower plot). In each plot, from top: real or imaginary parts of resistive wall contribution for a stainless steel beam pipe, an aluminum beam pipe, and a cold copper beam pipe. Lower curves: real and imaginary parts of the BPM contribution. All beam pipes are elliptical with radii 9 mm by 14 mm. One set of BPM striplines, either horizontal or vertical is assumed at each location of a FODO quadrupole. Each stripline is of length 8 cm subtending an angle of 30° at the center of the pipe.

Table 2: Collective instability limits of the VLHC bunches.

	PHASE 1		PHASE 2		
	Injection	Storage	Injection	Storage	
Beam pipe radii h/w	9/14	9/14	10/10	10/10	mm
Rf voltage V_{rf}	50	50	50	200	MV
Mode coupling limit $(Z_{\parallel}/n)_{\text{eff}}$	6.26	8.05	37.37	10.37	Ω
Mode coupling limit $(Z_{\perp})_{\text{eff}}$	112	576	1334	3245	M Ω /m
Resistivity of stainless steel ρ	$7.40 \cdot 10^{-7}$	$7.40 \cdot 10^{-7}$	$7.40 \cdot 10^{-7}$	$7.40 \cdot 10^{-7}$	Ω -m
Skin depth at $n = 1$, δ_1	1.20	1.20	1.20	1.20	cm
Wall imp. at $n = 1$, $[Z_{\parallel}/n]_1$	236	236	237	237	$(1+j) \Omega$
$[Z_{\perp}]_1$	$1.88 \cdot 10^5$	$1.88 \cdot 10^5$	$1.67 \cdot 10^5$	$1.67 \cdot 10^5$	$(1+j) \text{M}\Omega/\text{m}$
Re or $\text{Im}(Z_{\parallel}/n)_{\text{wall}}$ at rf freq	0.389	0.389	0.373	0.373	Ω
Voltage distortion	4.59	3.89	0.957	5.66	MV
Re or $\text{Im}(Z_{\parallel}/n)_{\text{wall}}$ at $m = 1$	0.267	0.278	0.291	0.187	Ω
Re or $\text{Im}(Z_{\perp})_{\text{wall}}$ at m_{eff}	521	543	592	380	M Ω /m
Power loss per unit length	0.703	0.610	0.062	0.235	W/m
Multi-bunch growth time	0.23	5.1	7.9	67.7	turns
Resistivity of aluminum ρ	$2.65 \cdot 10^{-8}$	$2.65 \cdot 10^{-8}$	$2.65 \cdot 10^{-8}$	$2.65 \cdot 10^{-8}$	Ω -m
Skin depth at $n = 1$, δ_1	0.23	0.23	0.23	0.23	cm
Wall imp. at $n = 1$, $[Z_{\parallel}/n]_1$	44.7	44.7	42.9	42.9	$(1+j) \Omega$
$[Z_{\perp}]_1$	$3.56 \cdot 10^4$	$3.56 \cdot 10^4$	$3.16 \cdot 10^4$	$3.16 \cdot 10^4$	$(1+j) \text{M}\Omega/\text{m}$
Re or $\text{Im}(Z_{\parallel}/n)_{\text{wall}}$ at rf freq	0.0736	0.0736	0.0706	0.0706	Ω
Voltage distortion	0.869	0.735	0.181	1.07	MV
Re or $\text{Im}(Z_{\parallel}/n)_{\text{wall}}$ at $m = 1$	0.0505	0.0527	0.0551	0.0353	Ω
Re or $\text{Im}(Z_{\perp})_{\text{wall}}$ at m_{eff}	98.5	103	112	71.8	M Ω /m
Power loss per unit length	0.133	0.115	0.012	0.044	W/m
Multi-bunch growth time	1.20	26.8	41.5	363	turns
Resistivity of copper ρ	$1.70 \cdot 10^{-8}$	$1.70 \cdot 10^{-8}$	$1.60 \cdot 10^{-9}$	$1.60 \cdot 10^{-9}$	Ω -m
Skin depth at $n = 1$, δ_1	0.018	0.018	0.056	0.056	cm
Wall imp. at $n = 1$, $[Z_{\parallel}/n]_1$	35.8	35.8	10.5	10.5	$(1+j) \Omega$
$[Z_{\perp}]_1$	$28.5 \cdot 10^3$	$28.5 \cdot 10^3$	$7.78 \cdot 10^3$	$7.78 \cdot 10^3$	$(1+j) \text{M}\Omega/\text{m}$
Re or $\text{Im}(Z_{\parallel}/n)_{\text{wall}}$ at rf freq	0.0589	0.0589	0.0173	0.0173	Ω
Voltage distortion	0.696	0.589	0.044	0.263	MV
Re or $\text{Im}(Z_{\parallel}/n)_{\text{wall}}$ at $m = 1$	0.0405	0.0422	0.0135	0.0087	Ω
Re or $\text{Im}(Z_{\perp})_{\text{wall}}$ at m_{eff}	78.9	82.3	27.5	17.7	M Ω /m
Power loss per unit length	0.106	0.092	0.0029	0.011	W/m
Multi-bunch growth time	1.5	33.4	161	1477	turns

the synchrotron sidebands are no longer equally separated with the m -th sideband at $\pm m\nu_s f_0$. The $m = 2$ sideband will move towards the $m = 1$ sideband as coupling impedance and/or bunch intensity increase. When the two sidebands merge into one, the $m = 1$ and $m = 2$ modes couple and an instability develops. This instability is not death threatening, stability will be regained after the bunch is lengthened and the energy spread increases. The threshold of the instability is given approximately by, for Gaussian distribution [3],

$$\left[\frac{\mathcal{I}m Z_{\parallel}}{n} \right]_{\text{eff}} \lesssim \frac{2\pi|\eta|E\sigma_E^2}{eI_{\text{pk}}} \quad (4.12)$$

where $I_{\text{pk}} = eN_b/(\sqrt{2\pi}\sigma_\tau)$ is the bunch peak current, and the effective impedance is

$$\left[\frac{\mathcal{I}m Z_{\parallel}}{n} \right]_{\text{eff}} = \frac{\int d\omega \frac{\mathcal{I}m Z_{\parallel}}{\omega} \omega_0 h_m(\omega)}{\int d\omega h_m(\omega)}, \quad (4.13)$$

and $h_m(\omega)$ the power spectrum of mode m and $\int d\omega$ implies discrete summation over all the m -th synchrotron sidebands. The longitudinal mode-coupling stability limits are listed in Table 2 for various situations of the VLHC operation. The instability will develop first near $m = 1$. Thus we evaluate the resistive wall impedance at $f_{(1)}$, with results shown in Table 2. We see that with a stainless steel beam pipe, the impedance Z_{\parallel}/n at $f_{(1)}$ in Phase 1 is only 0.267/0.278 Ω at injection/collision, and is very much lower than the stability limit of 6.26/8.05 Ω . Thus, no longitudinal mode-coupling instability will occur. The same is true for Phase 2.

Let us understand how the stability limit scales as the size of the accelerator ring increases. Notice that $|\eta| \sim \nu_\beta^{-2}$ in a FODO lattice and therefore scales as $|\eta| \propto R^{-1}$. Therefore, when the impedance of the ring is dominated by the resistive wall, the microwave stability criterion in Eq. (4.12) scales as, at a fixed frequency,

$$R^{1/2} \lesssim \frac{A\sigma_E}{RI_b} \propto \frac{A\sigma_E}{N_b}, \quad (4.14)$$

where Eq. (2.9) has been used. Thus the instability becomes worse as \sqrt{R} as the size of the ring increases.

5 TRANSVERSE MODE-COUPLING

With transverse motion, the $m = 0$ is a valid mode, which describes the bunch making rigid dipole oscillations in the transverse plane. This corresponds to just the pure betatron sidebands. Driven by the transverse impedance, the betatron tune decreases and the pure betatron sideband moves towards its first lower $m = -1$ synchrotron sideband. An instability will develop when the two overlap, which we call transverse mode-coupling instability (TMCI). Unlike the longitudinal counterpart, this instability is devastating. The growth time is usually small.

For an average bunch current I_b , the threshold of instability can be estimated by equating the downshift of the dipole betatron frequency to a synchrotron frequency. The threshold driving impedance is

$$[\mathcal{I}m Z_{\perp}]_{\text{eff}} \lesssim \frac{8E\omega_0^2\nu_{\beta}\nu_s\sigma_{\tau}}{eI_b c}, \quad (5.15)$$

where the effective transverse impedance is

$$[\mathcal{I}m Z_{\perp}]_{\text{eff}} = \frac{\int d\omega \mathcal{I}m Z_{\perp}(\omega) h_m(\omega)}{\int d\omega h_m(\omega)}, \quad (5.16)$$

and $\int d\omega$ implies discrete summation over the $m = 0$ synchrotron sidebands of the betatron tune lines (or just the betatron sidebands). These limits for various operations are listed in Table 2. It appears that the resistive wall impedance should be evaluated at frequency between $f_{(0)}$ and $f_{(1)}$, where the two modes collide. In fact, for a Gaussian bunch interacting with the resistive wall impedance, this effective frequency can be computed. Substituting the Gaussian spectrum and Eq. (2.7) into Eq. (5.16) gives

$$[\mathcal{I}m Z_{\perp}]_{\text{eff}} = \frac{[\mathcal{I}m Z_{\perp}]_1}{n_{\text{eff}}^{1/2}} \quad (5.17)$$

with

$$n_{\text{eff}} = \frac{4\pi}{\omega_0\sigma_{\tau}\Gamma^2(\frac{1}{4})} \quad \text{or} \quad f_{\text{eff}} = \frac{2}{\sigma_{\tau}\Gamma^2(\frac{1}{4})} = \frac{0.304}{2\sigma_{\tau}}, \quad (5.18)$$

where $\Gamma(\frac{1}{4}) = 3.63561$ is the Gamma function evaluated at $\frac{1}{4}$. This corresponds to $f_{(m_{\text{eff}})}$ with $m_{\text{eff}} = 0.304$ if Eq. (1.3) is used. For an aluminum beam pipe, which is used in the Phase 1 rings, the results as seen in Table 2 show that the threshold impedances are

98.5/102.7 M Ω /m at injection/collision, which are smaller than the stability limits of 125.7/643.9 M Ω /m. Thus, no transverse mode-coupling instability (TMCI) will occur and the safety factors are 1.27/6.26. For the Phase 2 rings where stainless steel beam pipes are used, the threshold impedances are 592/380 M Ω /m at injection/collision, which are less than the stability limits of 1492/3629 M Ω /m. The safety factors are 2.52/9.55.

The threshold of TMCI has been computed by Burov et al., [5] for the low-field VLHC bunches using a matrix approach by including 5 radial and 5 azimuthal modes and also verified by particle tracking. The resulting threshold at injection with the nominal set of parameters turns out to be only about half the designed intensity. After carefully examining the input parameters, it is concluded that the safety factor estimated from Eq. (5.15) appears to be $\sim 33\%$ larger than the result of Burov et al. Blaskiewicz [4] also solved the matrix equation to compute the threshold numerically for the high-field bunches and found the safety factor $\sim 1.7 \cdot 10^{10} / 0.910^{10} = 1.89$. Thus, there is a consistency that Eq. (5.15) always gives a threshold that is higher than that obtained from solving the coupling matrix by 30 to 40%. One source of discrepancy is related to the fact that the transverse coupling impedance driving the instability in the VLHC is dominated by the resistive wall rather than a broad band. The transverse resistive wake goes to infinity as the inverse square root of the distance between the source and the test particles, and this distance has been taken as the rms bunch length in the estimation using the simple formula of Eq. (5.15). On the other hand, the matrix approach brings up numerical convergence questions from the divergence of the wake at small distances. This discrepancy is very important for the low-field VLHC, because Burov's result points to an unstable bunch at injection while the estimate of Eq. (5.15) says that the bunch is just below the instability threshold. Even for the high-field bunches, the discrepancy lowers the safety limits significantly.

The high-field beam pipes are coated with a 50 μm layer of copper. The cold copper skin depth at the effective frequency at injection is only 1.76 μm . Thus only copper will be seen by the frequency components that take part in the transverse mode coupling. In other words, the safety factor should be very much enhanced.

As the size of the ring increases, the stability criterion of Eq. (5.15) scales as

$$R^{3/2} \lesssim \frac{\sqrt{R} \nu_s \sigma_\tau}{N_b} . \quad (5.19)$$

Thus, TMCI becomes worse as R . Comparing with Eq. (4.14), TMCI will have a lower threshold than the longitudinal microwave instability as the size of the ring increases.

5.1 BUNCH COALESCENCE

Facing the danger of TMCI of the low-field bunches at injection and the inability to estimate an accurate theoretical threshold, it is advisable to divide the bunch into a number of less intense bunches and perform a coalescence at a higher energy. In this section, we are going to estimate the rf voltage required for the coalescence.

A low-field VLHC bunch has an intensity of $2.5 \cdot 10^{10}$ particles in a $\omega_{\text{rf}}/(2\pi) = 478.0$ MHz rf bucket with rf harmonic $h = 369432$, corresponding to a ring circumference of $C = 231.7$ km. Assume that this bunch is divided into 5 bunches at consecutive buckets at injection. The coalescence operation consists of the following steps:

(1) The coalescence is to be performed at 20 TeV when the rf voltage is $V_{\text{rf}} = 50$ MV. The parameter lists supplied by Foster [1] call for a rms bunch area of 2.0 eV-s at storage. We therefore assume the rms bunch area of each bunch before coalescence be $A \sim 2.0/5 = 0.4$ eV-s, or a total bunch area $A_t \sim 2.4$ eV-s. The half energy spread and half width of the bunch are, respectively,

$$\begin{aligned} \left[\frac{\Delta E}{E} \right]_1 &= \sqrt{\frac{\omega_{s1} A_t}{\pi |\eta| E}} = 1.60 \cdot 10^{-4} , \\ [\Delta \tau]_1 &= \sqrt{\frac{|\eta| A_t}{\pi E \omega_{s1}}} = 0.239 \text{ ns} , \end{aligned} \quad (5.20)$$

where $\omega_{s1}/(2\pi)$ is the synchrotron frequency at the rf voltage $V_1 = 50$ MV and $\eta = 2.19 \cdot 10^{-5}$ is the slip factor.

(2) The rf voltage V_{rf} is snapped down to V_2 so that the bucket height is equal to the energy spread of the bunch. We have

$$\frac{eV_2}{E} = \frac{\pi |\eta| h}{2} \left[\frac{\Delta E}{E} \right]_1^2 = 3.23 \cdot 10^{-7} , \quad (5.21)$$

or $V_2 = 6.47$ MV.

(3) The bunch is allowed to rotate 90° with synchrotron frequency

$$\frac{\omega_{s2}}{2\pi} = \sqrt{\frac{|\eta| h e V_2}{2\pi E}} \frac{\omega_0}{2\pi} = 0.835 \text{ Hz} , \quad (5.22)$$

where $\omega_0/(2\pi) = 1.29$ kHz is the revolution frequency. The half energy spread becomes

$$\left[\frac{\Delta E}{E}\right]_2 = \frac{\omega_{s2}}{|\eta|} [\Delta\tau]_1 = 5.74 \cdot 10^{-5} . \quad (5.23)$$

(4) The rf is then turned off and the coalescence rf with a frequency of $478.0/9 = 53.11$ MHz ($h_c = h/9$) is turned on. The 5 bunches are rotated in the longitudinal phase space by 90° and the 478.0 MHz rf is then switched on to capture these bunches into one bucket. For total capture, the half energy spread $(\Delta E/E)_2$ of the bunches must rotate to a half width $(\Delta\tau)_c$ less than k times half a rf wavelength π/ω_{rf} , where $k < 1$. Notice that the phase equation of motion is

$$\frac{d\tau}{dt} = \eta \frac{\delta E}{E} . \quad (5.24)$$

We therefore require

$$[\Delta\tau]_c = \frac{|\eta|}{\omega_{sc}} \left[\frac{\Delta E}{E}\right]_2 \lesssim \frac{k\pi}{\omega_{\text{rf}}} , \quad (5.25)$$

where

$$\omega_{sc} = \omega_0 \sqrt{\frac{|\eta| h_c e V_c}{2\pi E}} \quad (5.26)$$

is the synchrotron frequency driven by the 53.11 MHz rf system at voltage V_c . The result is

$$\frac{eV_c}{E} \gtrsim \frac{h^2 |\eta|}{2\pi k^2 h_c} \left[\frac{\Delta E}{E}\right]_2^2 = \frac{1.53 \cdot 10^{-7}}{k^2} , \quad (5.27)$$

or $V_c \gtrsim 3.05 k^{-2}$ MV. The half energy spread of the coalesced bunch will be roughly 5 times the original multiplied by the factor k^2 , or

$$\left[\frac{\Delta E}{E}\right]_c \approx 5k^2 \left[\frac{\Delta E}{E}\right]_2 = 2.87 \cdot 10^{-4} k^2 . \quad (5.28)$$

The voltage of the captured rf at $h = 9h_c$ must be at least

$$V_4 = \frac{\pi h |\eta| E}{2e} \left[\frac{\Delta E}{E}\right]_{\text{coales}}^2 = \left(\frac{5k\pi}{6}\right)^2 V_c = 20.9 k^2 \text{ MV} . \quad (5.29)$$

The rf voltage is then raised to 50 MV adiabatically, so that the coalesced bunch, having a rms bunch area of roughly, 2 eV-s will have the designed bunch length for collision.

5.1.1 An ALTERNATE METHOD

In Step 3 of the coalescence, the synchrotron frequency is 0.834 Hz. Thus it takes 0.30 s for the bunch to rotate 90° and spread out. It is important to check whether longitudinal microwave instability will develop or not in this long duration. At the end of the spread, the bunch occupies the whole width of the bucket, which is $C/(ch) = 2.09$ ns, or a rms length of $\sigma_\tau \approx 0.427$ ns. The coalesced bunch should have a designed intensity of $2.48 \cdot 10^{10}$ particles. Before coalescence, the intensity of each bunch is 1/5 of it, or $N_b = 0.496 \cdot 10^{10}$, corresponding to a peak current $I_{\text{pk}} = eN_b/(\sqrt{2\pi}\sigma_\tau) = 0.742$ A. The Krinsky-Wang instability threshold is [3]

$$\frac{Z_{\parallel}}{n} = \frac{2\pi|\eta|E\sigma_E^2}{eI_{\text{pk}}} = 12.2 \Omega . \quad (5.30)$$

The resistive wall impedance for the VLHC beam pipe composing of stainless steel was found to be only $\text{Re } Z_{\parallel}/n = 0.389 \Omega$ at rf frequency. We can therefore conclude that longitudinal microwave instability will not occur.

Since we are far away from this instability, instead of snapping, one may also choose to reduce the 478.0 MHz rf voltage adiabatically in Step 2 so that the bunch fills the whole bucket. This method will lead to a lower energy spread before coalescence, and therefore a lower coalescence voltage in the 53.11 MHz rf. The lowest rf voltage required is

$$\frac{eV_2}{E} = \frac{\pi|\eta|h}{2} \left(\frac{h\omega_0 A_t}{8E} \right)^2 = 4.03 \cdot 10^{-8} , \quad (5.31)$$

or $V_2 = 0.8064$ MV. The half energy spread is the same as the bucket height, or

$$\left[\frac{\Delta E}{E} \right]_2 = \sqrt{\frac{2V_2}{\pi h|\eta|E}} = 5.63 \cdot 10^{-5} . \quad (5.32)$$

Step 3 is no longer necessary. We go to Step 4 where the coalescence rf is turned on to

$$\frac{eV_c}{E} \gtrsim \frac{9h|\eta|}{2\pi k^2} \left[\frac{\Delta E}{E} \right]_2^2 = \frac{1.47 \cdot 10^{-7}}{k^2} , \quad (5.33)$$

or $V_c \gtrsim 2.94 k^{-2}$ MV. The half energy spread is now

$$\left[\frac{\Delta E}{E} \right]_c \approx 5k^2 \left[\frac{\Delta E}{E} \right]_2 = 2.82 \cdot 10^{-4} k^2 . \quad (5.34)$$

The voltage of the captured rf at $h = 9h_c$ must be at least

$$V_4 = \frac{\pi h |\eta| E}{2e} \left[\frac{\Delta E}{E} \right]_{\text{coales}}^2 = \left(\frac{5k\pi}{6} \right)^2 V_c = 20.1k^2 \text{ MV} . \quad (5.35)$$

6 COUPLED-BUNCH INSTABILITY

The revolution frequencies of the VLHC rings are only 1.29 kHz. Thus the transverse resistive wall impedance at the betatron sideband of lowest negative frequency becomes very large and will drive a coupled-bunch instability.

For M_s identical equally spaced bunches in the ring, there are $\mu = 0, \dots, M_s - 1$ transverse coupled modes when the center of mass of one bunch lags behind its predecessor by the betatron phase of $2\pi\mu/M_s$. At the same time, each bunch can execute longitudinal motion with $m = 0, 1, \dots$ nodes. The growth rate for the μm -th mode is

$$\frac{1}{\tau_{\mu m}} = -\frac{1}{1+m} \frac{eMI_b c}{4\pi\nu_\beta E} \sum_k \text{Re } Z_\perp [(kM_s - \mu + \nu_\beta + m\nu_s)\omega_0] F'_m(\omega\tau_L - \chi) , \quad (6.36)$$

where M is the number of bunches. Strictly speaking Eq. (6.36) is correct only if $M = M_s$ or if the bunches are equally spaced. According to the 9-bucket spacing, the VLHC rings will be only 90% filled. Thus Eq. (6.36) will not be an accurate description of the beam dynamics.

As the frequency $\omega \rightarrow \pm 0$, the real part of the resistive-wall impedance approaches first $\pm|\omega|^{-1/2}$, then $|\omega|^{-1}$ when the skin depth exceeds the thickness of the pipe wall, and finally zero when the frequency is exactly zero. Therefore, there is always a mode μ that corresponds to a large negative $\text{Re } Z_\perp$ and drives the transverse coupled-bunch instability. For example, with the betatron tune $\nu_\beta = 214.4$, mode $\mu = 215$ or frequency $-0.6\omega_0/(2\pi) = 0.776$ kHz with $k = 0$ in the summation of Eq. (6.36) contributes the largest negative $\text{Re } Z_\perp$, which is $-5.63 \cdot 10^4$ M Ω /m if the Phase 1 beam pipe is of aluminum. Here, we stick to the $\pm|\omega|^{-1/2}$ dependency of the resistive wall impedance for simplicity, although at such a low frequency, the thickness of the beam pipe wall may be thinner than the skin depth. The next contribution with $k = 1$ will give $\text{Re } Z_\perp = +227$ M Ω /m which is negligibly small compared with the contribution at harmonic -0.6 , which therefore dominates the contribution.

The growth rates turn out to be extremely fast in all situations. The e -folding growth time is 1.2/27 turns for Phase 1 at injection/storage, where aluminum pipes

are considered. Correspondingly, the growth time for Phase 2 is 7.0/61 turns at injection/storage for stainless steel pipe. We use stainless steel because at a frequency less than 1 kHz, the influence of the 50 μm cold copper will be limited. Fortunately, the frequency of this mode is very low, around 1 kHz. A damper can be easily designed.

As the size of the accelerator ring increases, it is easy to show that the growth time in revolution turns scales as

$$\text{Growth time in turns} \propto \frac{N_b}{R}, \quad (6.37)$$

which explains why this transverse coupled-bunch instability driven by the resistive wall is so bad for the VLHC.

7 LONGITUDINAL HEAD-TAIL

Longitudinal head-tail instability has been observed in the Tevatron and we would like to examine its effect in the VLHC. This instability is a result of the asymmetric dependence of the momentum compaction factor $\alpha = \alpha_0(1 + \alpha_1\delta) + \dots$ on the momentum deviation δ . Thus, a bunch will have slightly different length and therefore lose energy differently in the upper and lower halves of the longitudinal phase space. The growth rate of the synchrotron oscillation amplitude is given by

$$\frac{1}{\tau} = -\frac{f_0}{2} \frac{dU}{d\sigma_\tau} \frac{\sigma_\tau}{E} \chi, \quad (7.38)$$

where the energy loss per particle per turn is

$$U(\sigma_\tau) = e^2 N \int d\omega |\tilde{\rho}(\omega)|^2 \text{Re} Z_{\parallel}(\omega), \quad (7.39)$$

and

$$\chi = \frac{\alpha_0(\alpha_1 - \eta + \frac{3}{2})}{\eta} \approx \alpha_1 + \frac{3}{2} \quad (7.40)$$

denotes the asymmetry, which is roughly 2 since $\alpha_1 \approx \frac{1}{2}$ for a FODO lattice.

The instability can be driven by a sharp resonance like the fundamental mode of the rf cavities. For the Tevatron, the quality factor $Q \approx 7000$ and the shunt impedance

is $R_s = 1.2 \text{ M}\Omega$. Here, for the VLHC, it is reasonable to assume Q to be the same while $R_s/Q = 1710$, about 10 times larger. Thus, the growth rate of Eq. (7.38) scales as

$$\frac{1}{\tau} \propto \frac{1}{RE} \propto \frac{1}{R^2}. \quad (7.41)$$

Thus, we expect the growth rate to be very small for the VLHC. As shown in Table 3, these growth rates are very much less than $86400^{-1} = 1.15 \cdot 10^{-5} \text{ s}^{-1}$, implying that there will not be any appreciable growth of the synchrotron amplitude in a day. The small growth rates are a result of the low rf frequency and short bunch length, which represents a point on the upper plot of Fig. 2. to the very left of the $-dU/d\sigma_\tau)\sigma_\tau$ peak.

The longitudinal head-tail instability can also be driven by a broad-band resonance of the coupling impedance. If we assume $Z_{||}/n \approx 1$ does not change much with the size of the ring, R_s/Q will increase as the radius R of the ring. Thus, the growth rate driven by the broad-band impedance scales as

$$\frac{1}{\tau} \propto \frac{1}{E} \propto \frac{1}{R}, \quad (7.42)$$

and will dominate the growth driven by the sharp resonance of the rf cavities. The lower plot in Fig. 2 gives the reduced differential energy loss, $(dU/d\sigma_\tau)\sigma_\tau$ as a function of $f_r\sigma_\tau$ with f_r denoting the frequency of the broad-band.

The growth rates driven by a broad-band impedance at various frequencies are listed in Table 3. For the injection into the low-field rings, all growth rates from the table exceed $3600^{-1} = 2.78 \cdot 10^{-4}$ or with growth time less than an hour. Unfortunately, the injection into the low-field rings is slow and is about an hour. Thus there will be significant growth of the synchrotron amplitude and thus the bunch area. However, there will not be any influence on the high-field rings at injection because that injection takes less than 30 s.

At storage, the growth rates are $6.44 \cdot 10^{-4}$ and $4.52 \cdot 10^{-5} \text{ s}^{-1}$, respectively, for Phase 1 and Phase 2 when $f_r = 3 \text{ GHz}$ and $Q = 1$, or growth times of 4.31 and 6.15 hours. These numbers appear to be insignificant for a store that lasts up to 10 hours. However, if the resonant frequency is reduced, the growth rate will increase, which corresponds to moving towards the peak of the $-(dU/d\sigma_\tau)\sigma_\tau$ plot from the right side in the lower plot of Fig. 2. As indicated in Table 3, when $Q = 1$ and $f_r = 1 \text{ GHz}$, the growth time reduces to 1.79 hours for Phase 1 and becomes significant. On the other hand, the growth rate for Phase 2 storage decreases instead as f_r decreases, which is because $f_r\sigma_\tau$ has become

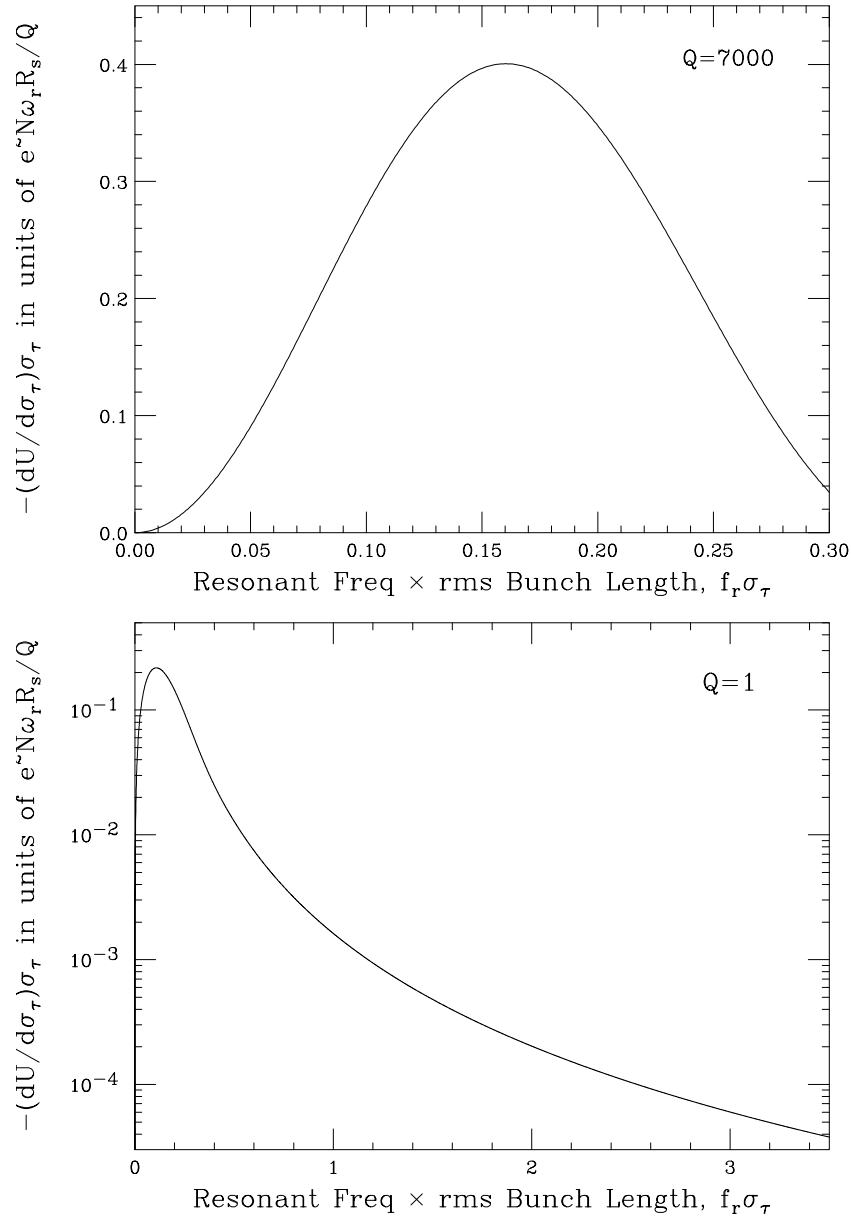


Figure 2: Plot of differential bunch energy loss $(dU/d\sigma_\tau)\sigma_\tau$ versus $f_r\sigma_\tau$ due to a sharp resonance (upper) or a broad-band impedance (lower).

Table 3: Parameters of the VLHC ring in Phase 1 and Phase 2, at injection and storage modes.

	PHASE 1		PHASE 2		
	Injection	Storage	Injector	Storage	
Driven by rf resonance					
$f_{\text{rf}} = 477.9 \text{ MHz}, R_s/Q = 1710 \text{ } \Omega, Q = 7000$					
Growth rates	$7.77 \cdot 10^{-6}$	$3.89 \cdot 10^{-7}$	$3.39 \cdot 10^{-7}$	$1.03 \cdot 10^{-8}$	s^{-1}
Driven by broad-band with $R_s/n = 1.0 \text{ } \Omega$					
Growth rates ($f_r = 3 \text{ GHz } Q = 1$)	$1.84 \cdot 10^{-3}$	$6.44 \cdot 10^{-5}$	$2.78 \cdot 10^{-5}$	$4.52 \cdot 10^{-5}$	s^{-1}
Growth rates ($f_r = 2 \text{ GHz } Q = 1$)	$2.72 \cdot 10^{-3}$	$9.54 \cdot 10^{-5}$	$4.25 \cdot 10^{-5}$	$5.35 \cdot 10^{-5}$	s^{-1}
Growth rates ($f_r = 1 \text{ GHz } Q = 1$)	$3.96 \cdot 10^{-3}$	$1.55 \cdot 10^{-4}$	$7.76 \cdot 10^{-5}$	$2.26 \cdot 10^{-5}$	s^{-1}
Growth rates ($f_r = 1 \text{ GHz } Q = 2$)	$2.85 \cdot 10^{-3}$	$1.09 \cdot 10^{-4}$	$4.88 \cdot 10^{-5}$	$1.35 \cdot 10^{-5}$	s^{-1}
Driven by resistive wall					
Resistivity of stainless steel ρ	$7.40 \cdot 10^{-7}$	$7.40 \cdot 10^{-7}$	$7.40 \cdot 10^{-7}$	$7.40 \cdot 10^{-7}$	$\Omega\text{-m}$
Growth rate	$2.44 \cdot 10^{-4}$	$9.71 \cdot 10^{-6}$	$5.43 \cdot 10^{-6}$	$2.36 \cdot 10^{-6}$	s^{-1}
Resistivity of aluminum ρ	$2.65 \cdot 10^{-8}$	$2.65 \cdot 10^{-8}$	$2.65 \cdot 10^{-8}$	$2.65 \cdot 10^{-8}$	$\Omega\text{-m}$
Growth rate	$4.63 \cdot 10^{-5}$	$1.84 \cdot 10^{-6}$	$1.03 \cdot 10^{-6}$	$4.45 \cdot 10^{-7}$	s^{-1}
Resistivity of copper ρ	$1.70 \cdot 10^{-8}$	$1.70 \cdot 10^{-8}$	$1.60 \cdot 10^{-9}$	$1.60 \cdot 10^{-9}$	$\Omega\text{-m}$
Growth rate	$3.71 \cdot 10^{-5}$	$1.47 \cdot 10^{-6}$	$2.53 \cdot 10^{-7}$	$1.10 \cdot 10^{-7}$	s^{-1}

so small that it goes past the peak of the $-(dU/d\sigma_\tau)\sigma_\tau$ plot. It is also shown in the table that the growth rate will drop if the quality factor Q increases.

The longitudinal head-tail instability can also be driven by the resistive wall impedance. The differential energy loss in Eq (7.40) integrates to

$$\frac{dU}{d\sigma_\tau} \sigma_\tau = -\frac{3\Gamma(\frac{3}{4})}{8\pi^2} \frac{e^2 N_b [\text{Re } Z_{\parallel}]_1}{\omega_0^{1/2} \sigma_\tau^{3/2}}, \quad (7.43)$$

where $[\text{Re } Z_{\parallel}]_1$ is the resistive part of the wall impedance at revolution frequency. The results in Table 3 show that this instability is insignificant. For example, at the injection of Phase 1, the growth time for the aluminum pipe is longer than the one hour injection time. At storage, the growth times are tens of hours for both phases. However the growth rate is inversely proportional to $\sigma_\tau^{3/2}$. Therefore, when the bunch length is further shortened in future design or operation, longitudinal head-tail instability driven

by the resistive wall impedance may become important.

8 OTHER ISSUES

We have not studied all types of instability. There are many bunches in the collider ring. Therefore, coupled-bunch instabilities in both the longitudinal and transverse planes by sharp resonances can be serious, and an investigation is required. The beam pipe has a small bore. As a result, the image contribution to the coherent and incoherent betatron tune shifts can be important

Also one should have a more thorough study of the impedance budget of the collider ring, and see whether contribution from sources other than resistive wall is truly unimportant.

APPENDIX BPM

With a betatron tune of 214, there will be 828 90° FODO in each of the VLHC rings. If a set of beam position monitors (BPMs) is installed at each quadrupole, there will be $M = 1656$ sets of beam position monitors in each VLHC ring, half of them detect horizontally and half vertically. Similar to the Tevatron, we assume each set of BPMs to be a pair of 2 cylindrical strip-lines of radius $b = 0.9$ cm, each subtending an angle[‡] $\phi_0 = 30^\circ$ at the center of the beam pipe and is of length[§] $\ell = 8$ cm. Each stripline is terminated at both ends and forms a transmission line of characteristic impedance $Z_c = 50 \Omega$ with the beam pipe wall that bulges out. The longitudinal and transverse coupling impedances have been calculated to be

$$Z_{\parallel} = 2MZ_c \left(\frac{\phi_0}{2\pi} \right)^2 \left(\sin^2 \frac{\omega\ell}{c} + j \sin \frac{\omega\ell}{c} \cos \frac{\omega\ell}{c} \right), \quad (\text{A.44})$$

[‡]The VLHC bunches are very much intense than the anti-proton bunches in the Tevatron. Therefore we assume a smaller covering angle of $\phi_0 = 30^\circ$ than the $\phi_0 = 110^\circ$. In fact, this angle can further be reduced. For simplicity, we assume the VLHC beam pipe to be cylindrical here.

[§]The bunches are very much shorter here. Therefore we shorten the Tevatron stripline from 18 cm to 8 cm.

$$Z_{\perp} = \frac{c}{2b^2} \left(\frac{4}{\phi_0} \right)^2 \sin^2 \frac{\phi_0}{2} \frac{Z_{\parallel}}{\omega}, \quad (\text{A.45})$$

where the factor $\frac{1}{2}$ is inserted in the expression for Z_{\perp} because one half of the BPM sets work for the horizontal and one half for the vertical. At low frequencies, the impedances are inductive,

$$\begin{aligned} \frac{Z_{\parallel}}{n} &= j 2M Z_c \left(\frac{\phi_0}{2\pi} \right)^2 \frac{\ell}{R} = j 0.0025 \Omega, \\ Z_{\perp} &= j 2.22 \text{ M}\Omega/\text{m}. \end{aligned} \quad (\text{A.46})$$

The small $\mathcal{I}m Z_{\parallel}/n$ at low frequencies is expected. Since the betatron function increases as the square root of the ring circumference C , $\mathcal{I}m Z_{\parallel}/n$ should fall inversely as \sqrt{C} and also the length of the striplines. $\mathcal{I}m Z_{\perp}$ at low frequencies scales as \sqrt{C} and b^{-2} according to Eq. (A.45). Notice that $\mathcal{I}m Z_{\parallel}/n$ at low frequencies is independent of the size of the beam pipe. At high frequencies, the reactive parts of the impedances oscillate between inductive and capacitive; for example, the first zero occurs when $f = c/(4\ell) = 0.937$ GHz. The real parts rise from zero quadratically with frequency and $\mathcal{R}e Z_{\parallel}/n$ has a peak value of 0.0018Ω at 0.695 GHz.

References

- [1] W. Foster, *Staged VLHC Parameter List Version 0.4 2/23/01*, private communication.
- [2] See for example, K.Y. Ng, *Impedances and Collective instabilities of the Tevatron at Run II*, Fermilab Report TM-2055, 1998.
- [3] S. Krinsky and J.M. Wang, *Particle Accelerators* **17**, 109 (1985).
- [4] M. Blaskiewicz, *Stability issues for the high field VLHC*, this workshop.
- [5] A. Burov et al., *Nucl. Instrum. Meth.* **A450**, 194 (2000).